RSC Advances

PAPER

View Article Online
View Journal | View Issue

Cite this: *RSC Adv.*, 2017, **7**, 10479

Moldable clay-like unit for synthesis of highly elastic polydimethylsiloxane sponge with nanofiller modification†

Shi Qiu,[a] Hengchang Bi,[a] Xiaohui Hu,[a] Mingbo Wu,*[b] Yongfeng Li[c] and Litao Sun*[a]

Received 12th November 2016
Accepted 24th January 2017

DOI: 10.1039/c6ra26701g

rsc.li/rsc-advances

Polydimethylsiloxane (PDMS) sponges with nanofiller modification are gaining considerable attention because of their extraordinary performances in improving the qualities of polymer nanocomposites. However, the current synthesis methods limit the flexibility and stability of functional PDMS sponges. Herein, we present an ultrasound-assisted *in situ* polymerization approach to convert a novel clay-like PDMS nanocomposite into a functional PDMS sponge. Accessible ultrasound with low intensity can moderately regulate the cross-linking degree of PDMS oligomer to obtain only shape-controllable clay-like units for the scalable synthesis of a PDMS sponge with a high elasticity. In order to enhance the functionality, graphene nanosheets serve as a nanofiller uniformly distributed into the three-dimensional porous PDMS skeleton. The graphene-reinforced PDMS sponge (GRPS) exhibits mechanical stability and wettability, and is a better alternative to typically recyclable adsorbents in an oil–water separation system. Thus, the present synthesis method may pave a facile way for manufacturing functional PDMS sponges on a large scale.

Introduction

Polydimethylsiloxane (PDMS), comprising repeated units of –O–$Si(CH_3)_2$–,[1] is the most commonly used silicone-based elastomer, due to its transparency, viscoelasticity, dielectricity, hydrophobicity, biocompatibility, and scalability,[2] and it has become a crucial material in many kinds of applications, including microfluidic devices,[3] wearable electronics,[4] capacitive sensors,[5] tissue engineering scaffolds,[6] and waterproof membranes.[7,8] Particular interest has focused on the synthesis of a three-dimensional porous PDMS architecture serving as a new paradigm for oil adsorbents,[9] nanogenerators,[10] and soft robotics,[11] using salt, sugar, and sodium bicarbonate as the fugitive porogen. In the present study, a solvent evaporation approach has been developed to fabricate porous skeletons *via* vacuum[12] or air blow,[13] which can achieve the encapsulation of a template with a PDMS matrix through capillary forces. However, the vacuum operation at extreme pressure and temperature limits the elasticity of the as-made PDMS sponges. Although the introduction of a volatile organic solvent can adjust the elasticity of the porous PDMS skeletons produced by the lightly cross-linked PDMS oligomers, the unalterable shape of the products also limits the diversified application of PDMS sponges. Therefore, the development of a simple and flexible synthetic strategy presents a major challenge.

Inorganic–organic composites are an innovative class of polymeric materials, which can coordinate the functionality of an inorganic nanomaterial and the elasticity of an organic polymer matrix. PDMS sponges incorporated with nanofillers, such as $BaTiO_3$ nanoparticles,[14] TiO_2 nanoparticles,[15] carbon nanotubes,[16] graphene nanosheets,[17] and metals[18] have attracted great interest with regard to their practical applications, because they are known to reinforce piezoelectric, photoresponsive, mechanical, wetting and conductive properties, respectively. In order to form polymer nanocomposites, a dip coating method is used to perform the nanofiller deposition on the surface of PDMS sponges prepared beforehand.[15,16] However, the van der Waals force is a relatively weak interaction between the nanofiller and porous PDMS skeleton, leading to mechanical instability under compression, stretch, twist, and friction conditions. Thus, the loose interaction between nanofiller and PDMS matrix is crucial for their industrial applications. Recently, an *in situ* polymerization method has been developed to address the weak linkage, resulting in three-dimensionally cross-linked networks between the nanofiller and the PDMS matrix.[19] However, this approach is still a roughly mechanical mixture, which hinders the uniformity of the composite structure and hampers the performances of functional PDMS sponges in practical applications.

[a]*SEU-FEI Nano-Pico Center, Key Laboratory of MEMS of Ministry of Education, Southeast University, Nanjing, 210096, P. R. China. E-mail: slt@seu.edu.cn*

[b]*CPCIF Key Lab for Carbon Materials from Heavy Oil, State Key Laboratory of Heavy Oil Processing, China University of Petroleum, Qingdao, 266580, P. R. China. E-mail: wumb@upc.edu.cn*

[c]*State Key Laboratory of Heavy Oil Processing, China University of Petroleum, 102249, Beijing, P. R. China*

† Electronic supplementary information (ESI) available. See DOI: 10.1039/c6ra26701g

To address these limitations, herein we report an ultrasound-assisted *in situ* polymerization approach to convert a moldable clay-like PDMS nanocomposite into a functional PDMS sponge. Graphene nanosheets act as a nanofiller, PDMS as a matrix, and sea salt crystals as a template. Accessible ultrasound with low intensity can regulate the moderately cross-linked PDMS oligomer to obtain only a shape-controllable clay-like graphene–PDMS–salt unit, which is especially applicable for the scalable synthesis of a graphene-reinforced PDMS sponge (GRPS). As a result, GRPSs show high flexibility and strong hydrophobicity, and can be used as a recyclable adsorbent in an oil–water separation system. Thus, this work opens up a new avenue for the efficient production of elastic PDMS sponges with functionality *via* the moldable clay-like unit.

Experimental

Preparation of clay-like units and GRPSs

The scalable production of graphene nanosheets *via* shear-assisted supercritical CO_2 exfoliation was described elsewhere in the literature.[20] For ultrasound-assisted *in situ* polymerization, liquid PDMS (1 g of base agent with 0.1 g of curing agent of Sylgard 184 and 10–40 mL of EtOAc), graphene (0–40 mg), and a certain volume of salt particles (10 g) were added into a reaction vessel and placed in an ultrasonic cleaning bath. During the EtOAc evaporation, the clay-like graphene–PDMS–salt units were obtained. Then, these composites were molded into desired shapes and cured at 60–90 °C overnight. Hard and nonviscous composites were immersed in hot water to leach out the salt crystal templates. After drying, GRPS-*x* with 0–4 wt% of graphene contents was finally obtained; where, *x* is defined as the mass percentage of graphene loading content to PDMS matrix.

Characterization

GRPS microstructures were observed *via* SEM (Hitachi S4800, Japan) and TEM (EOL JEM-2100, Japan). Salt particle sizes were characterized using a polarizing microscope (Nanjing Jiangnan Novel Optics XPL-2, China). Raman scattering measurements were carried out with a Raman spectrometer (Renishaw inVia Reflex, UK). Water contact angles were measured with an optical contact-angle meter (Kruss DSA-100, Germany). Compression tests were measured using a force gauge (Mark-10 series 5, USA) equipped with a 10 N load cell at a constant loading and unloading speed of 200 mm min^{-1}. The sample geometry used for compression tests was 2.5 cm (diameter) × 3.0 cm (height). Bending tests were measured using a two-phase stepping motor (TOPCNC 86BYG68A, China). The sample dimension was 3.0 cm (diameter) × 0.3 cm (height).

Solvent and oil adsorptions of GRPSs

In a typical adsorption test, GRPS was immersed into corresponding organic liquids for a set time and then picked out for measurement. The specimens for adsorption tests were made into cubic blocks 3.0 cm × 3.0 cm × 3.0 cm. The weights of the GRPS before (m_o) and after (m_t) adsorption were recorded to estimate the adsorption capacity (q). The q values were calculated from the following formula:

$$q = (m_t - m_o)/m_o \times 100\%$$

Each organic liquid was tested for five cycles. Subsequently, the adsorption kinetics of GRPS were investigated by quantifying the adsorbed *n*-hexane as a function of contact time with a time interval of 1 s. The recyclability was evaluated by the cyclic adsorption–squeeze measurement.

Results and discussion

Fig. 1 schematically illustrates the ultrasound-assisted *in situ* polymerization approach for incorporating graphene into salt-template-derived PDMS nanocomposites. Commercial sea salt crystals were selected to act as a template, with an average size of 650 μm (Fig. S1, ESI†). A perfect graphene nanosheet is hydrophobic in nature,[21] and exhibits exceptional mechanical stiffness.[22,23] To improve the performance of the initial PDMS sponge as much as possible, graphene nanosheets served as a nanofiller fabricated by the shear-assisted supercritical CO_2 exfoliation method,[20] exhibiting thin and transparent sheets according to transmission electron microscopy (TEM) characterization (Fig. 1a). The graphene nanosheets comprise 5 to 10 monolayers per sheet, as observed by high-magnification TEM (the inner of Fig. 1a) and Raman spectroscopy (Fig. 1b) analyses.

Ultrasound is a unique means of interaction between energy and matter,[24] and it arises from acoustic cavitation: the formation, growth, and implosive collapse of bubbles in liquids, leading to intense local heating, high pressure, and very short lifetimes.[25] It can release enough kinetic energy from the generation of localized hot spots to activate various chemical reactions to completion, even some reactions that were previously difficult to realize by other traditional methods.[26] Therefore, an ultrasound-assisted *in situ* polymerization approach was explored as a modified method. Three functions of ultrasound were involved in the fabrication of the clay-like unit. First, under continuous ultrasonic irradiation, the physical effect induced by cavitation bubbles can first accelerate graphene dispersion into the solution, increasing the possibility of collision between the graphene nanofiller and the PDMS matrix. Second, the polymerization process of PDMS is mainly through a hydrosilylation reaction between vinyl (–CH=CH_2) end groups of the PDMS prepolymer and Si–H groups of the PDMS cross-linker in the presence of platinum-based catalysts.[27] As a result, the platinum-based catalyst which served as one component of the PDMS can be activated by the thermo-mechanical energy arising from the ultrasonic effect,[28,29] improving the catalytic efficiency of the hydrosilylation reaction with regard to the polymerization of the PDMS oligomer. Third, the moderately cross-linked polymer can uniformly and efficiently coat on the salt crystal surface, leading to a graphene–PDMS–salt composite.

It is worth noting that the ultrasound-assisted *in situ* polymerization, which is done under an accessibly ultrasonic

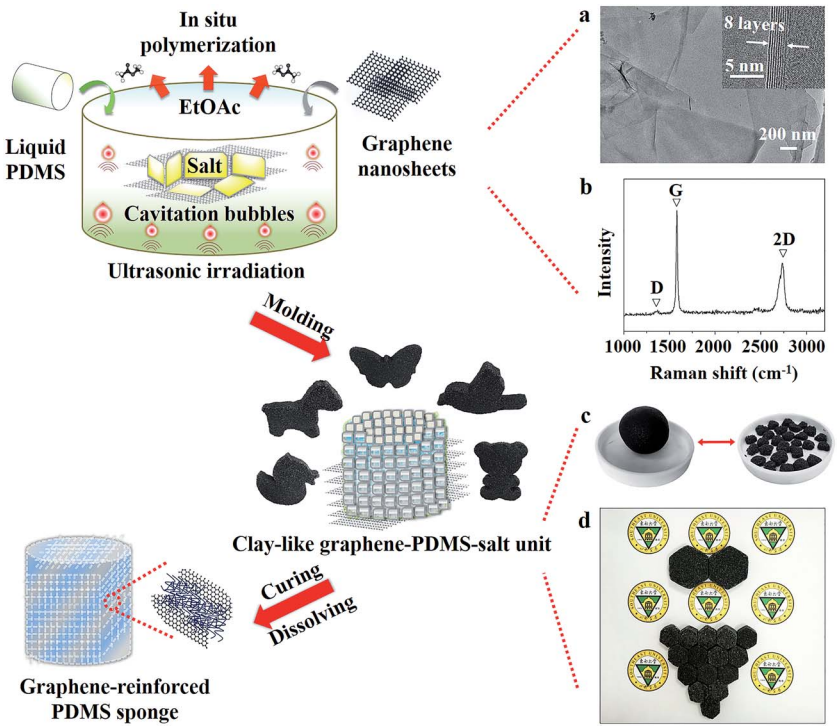

Fig. 1 Schematic illustration of the ultrasonic synthesis of moldable clay-like units for scalable production of GRPSs. (a) TEM and the corresponding HRTEM images of graphene nanosheets. (b) Raman spectrum of graphene. (c and d) Digital photographs of various macroscopic features of clay-like units.

cleaning bath with a low intensity ($\sim$1 W cm^{-2}), can regulate the moderately cross-linked PDMS oligomer to obtain only clay-like units. The primary benefit of this approach is that it does not produce the completely cross-linked PDMS oligomer that has limited the elasticity and shape diversity of products based on the traditional solvent evaporation methods.[19] Therefore, these novel composites can be molded into any desired shapes *via* the viscoelasticity of the clay-like units, which are similar to Silly Putty. As shown in Fig. 1c, the irregular small clay-like units are assembled into a large spherical shape and arbitrary sizes of hexagons; these hexagons can also be arranged into desired polygons (Fig. 1d). After curing of the graphene–PDMS–salt composites, GRPSs with high flexibility were readily obtained by immersing the composites in hot water, dissolving the salt component and leaving the three-dimensional macropore skeleton. Unlike typical synthetic methods (Table S1, ESI†), the ultrasound approach obviously simplifies complex synthetic steps, and results in a kind of novel clay-like unit, making possible the scalable production of highly elastic PDMS sponges with a nanofiller modification.

Fig. 2a shows the cylindrical shapes of as-made GRPSs obtained from clay-like units, and the change in color from white to black with an increasing graphene content. Interestingly, GRPSs can be easily manipulated into rolls without structural damage from originally flat or columnar shapes (Fig. 2b and c and Movie S1, ESI†), similar to superelastic graphene/polyimide nanocomposite foams.[30] Hence, we performed a systematic mechanical testing on GRPSs to investigate their compressibility and recoverability. Fig. 2d presents the compressive

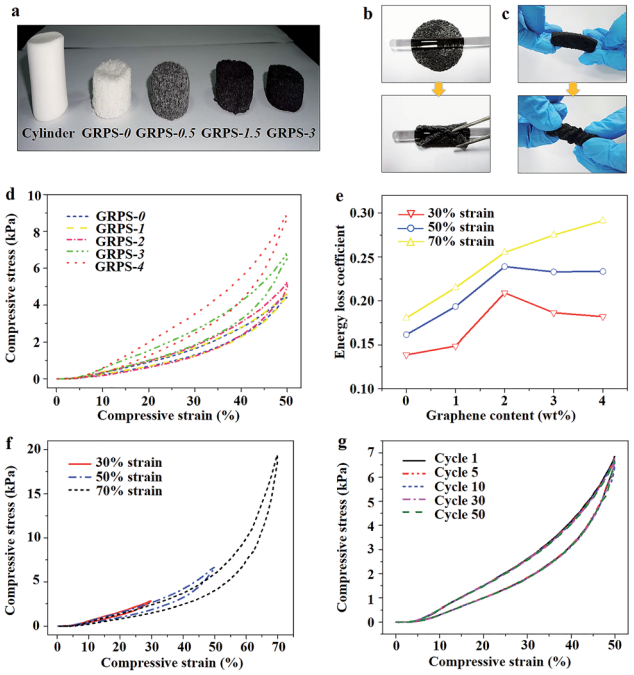

Fig. 2 Mechanical behaviors of GRPSs. (a) Digital photograph showing a cylinder and a series of cylindrical GRPSs with different graphene contents. (b and c) Transformation of the GRPS-*3* scaffolds into curly shapes. (d) Compressive stress–strain curves of GRPSs at 50% strain deformation. (e) The relationship between energy loss coefficient and graphene content at different strain deformations. (f) Compressive stress–strain curves of GRPS-*3* at various set strains of 30%, 50%, and 70%, respectively. (g) Cyclic stress–strain curves of GRPS-*3* at 50% strain deformation.

stress–strain curves of GRPSs (up to 50% strain). The initial linear elastic regions of GRPSs reached 30% strain deformation, which is superior to the previous PDMS sponges reported by a sugar-templating approach (15–20%).[31] Both ultimate strength and Young's modulus of GRPSs have been enhanced by the incremental graphene contents (Fig. S2a and Table S2, ESI†). The measured Young's moduli of GRPSs were approximately 5.83–14.14 kPa, which are in agreement with the pristine PDMS sponges (5.56–20 kPa) and much lower than those of reported PDMS sponges with nanofiller modification (100–169 kPa) (Table S1, ESI†). As a result, this ultrasound approach can address limitations of the flexibility of PDMS nanocomposites. Fig. 2e shows the relationship between the energy loss coefficients of GRPSs and the graphene loading contents at different strain deformations. The values of energy loss coefficients were in the range of 0.14 to 0.29, indicating low energy dissipation in contrast to typically compressible graphene aerogels (0.75–0.83).[32,33] The energy dissipation of GRPSs quickly increased with the rise in strain amplitude, owing to the incremental frictions between flowing air and the sponge skeleton.[34,35] Obvious turning points in the corresponding energy loss coefficients appeared in GRPS-*2* (below 50% strain amplitude), which might be related to the changing trends in ultimate strength and elastic modulus with different graphene content (Fig. S2a, ESI†). When graphene loading content was maintained at the level of 2–4 wt%, the reinforced mechanical stability of GRPSs could protect them from structural damage from external compression, resulting in a reduction in energy dissipation. However, it is difficult to obtain a porous skeleton from a 5 wt% graphene loading content, which means that an excess of graphene nanofiller may interrupt the cross-linked PDMS matrix.

Thus, we selected GRPS-*3* to study cyclic compression behaviors. The stress–strain curves of GRPS-*3* at different strain deformations of 30%, 50%, and 70% were investigated (Fig. 2f). Each succeeding loading curve returned to the preceding cycle and continued the trend of the preceding loading curve, thereby displaying a shape memory characteristic along a given loading path.[36] Then, stress responses were measured at a constant stress amplitude (50% strain deformation) as a function of cycle number (Fig. 2g). The cyclic stress–strain curves of GRPS-*3* show that the areas of the hysteresis loops remain constant and avoid stress-softening behavior. In addition to the recyclable compressibility, GRPS-*3* underwent bending fatigue for at least 30 000 cycles (Movie S2, ESI†). Thus, the excellent elasticity deformation restorability of GRPS-*3* is superior to reported graphene-based sponges with high oil adsorption capacity (Experiment S1, Fig. S2b and Movie S1, ESI†).[37,38] The notable mechanical performances are very important in the recyclability of adsorbents and the recoverability of pollutants in practical applications.

The microstructures of GRPSs were investigated *via* scanning electron microscopy (SEM) characterization. The top surfaces of GRPSs exhibit dense and compact structures, demonstrating no apparent differences between GRPS-*0* and GRPS-*3* (Fig. S3, ESI†). Then, when GRPSs were sliced, three-dimensionally interconnected macroporous networks emerged on the fracture surfaces, displaying a shallow bowl-shape morphology (Fig. 3a and c). In contrast to the irregular pore structure of the reported PDMS-based sponges, GRPSs show a narrow pore-size distribution of cellular holes with an average diameter of 630 μm, which are in agreement with the sizes of commercial salt crystals. It is noted that the incremental graphene contents of GRPSs can form diverse morphologies on cellular hole surfaces, especially the more crumpled pore walls of GRPS-*3* (Fig. 3c) compared to GRPS-*0* (Fig. 3a). These phenomena were observed clearly through the high magnification of SEM images. Unlike the relatively smooth topography of the original PDMS sponge (Fig. 3b), Fig. 3d presents cuticular folds of GRPS-*3* with a strip width from 540 nm to 1.54 μm, demonstrating the microstructural change in GRPSs from incorporating a graphene component. Furthermore, the results could be supported by the corresponding Fourier transform infrared spectroscopy (FTIR) spectra (Fig. S4, ESI†). The obvious decrease in the intensity of the absorption bands of GRPS-*3* (at 802 cm^{-1} and 1262 cm^{-1} due to Si–CH_3 vibration, 2905 cm^{-1} and 2965 cm^{-1} due to the symmetric and asymmetric stretching vibrations of C–H in methyl groups)[39] indicates that graphene nanosheets have been embedded into the interior of the PDMS elastomer and tightly covered the entire surface of the porous skeleton. As a consequence, the unique microstructures of GRPSs might result in a functional integration between the graphene nanofiller and the PDMS matrix for surface modification.

Owing to bioinspired surfaces, the cooperative interactions of multiscale structures and chemical compositions have been demonstrated to form a fascinatingly wetting surface.[40] The relationship between the wetting behaviors of as-made GRPSs and different graphene loading contents was investigated. Fig. 3e shows a water contact angle (WCA) of 140° on the outside surface of GRPS-*0* and a WCA of 146° on the inner surface of GRPS-*0*, which are in agreement with the previous reports of hydrophobic PDMS sponges.[9] With a graphene loading up to 3 wt%, the WCAs of GRPS-*3* on the outside surface and inner surface reached 149° and 151°, respectively. It is known that the surface wettability can be enhanced by being textured with different scale structures. Therefore, the superhydrophobicity of GRPS-*3* can be attributed to the multiscale structure depending on the cellular holes in the microscale and cuticular folds in the nanoscale by the cooperative interactions of the graphene nanofiller and the PDMS matrix.

According to the "petal effect",[41] this multiscalar structure of GRPS-*3* is expected to produce another superhydrophobic surface: the Cassie impregnating wetting state.[42] As shown in Fig. 3f, a water droplet (5 μL) was not easily dragged back by the needle when it came into slight contact with the GRPS-*3* surface (Movie S3, ESI†). This result suggests a highly adhesive surface for GRPS-*3*, which is consistent with the sticky superhydrophobicity of a graphene aerogel at low surface tension modification.[43] As to the multiscalar structure of GRPS-*3*, water droplets are able to enter into the cellular holes of the surface but not into the cuticular folds, resulting in a large contact angle and a high contact angle hysteresis. Thus, this special petal-like property of GRPS-*3* has potential application in liquid transportation without loss.[44] Fig. 3g shows how a small-volume

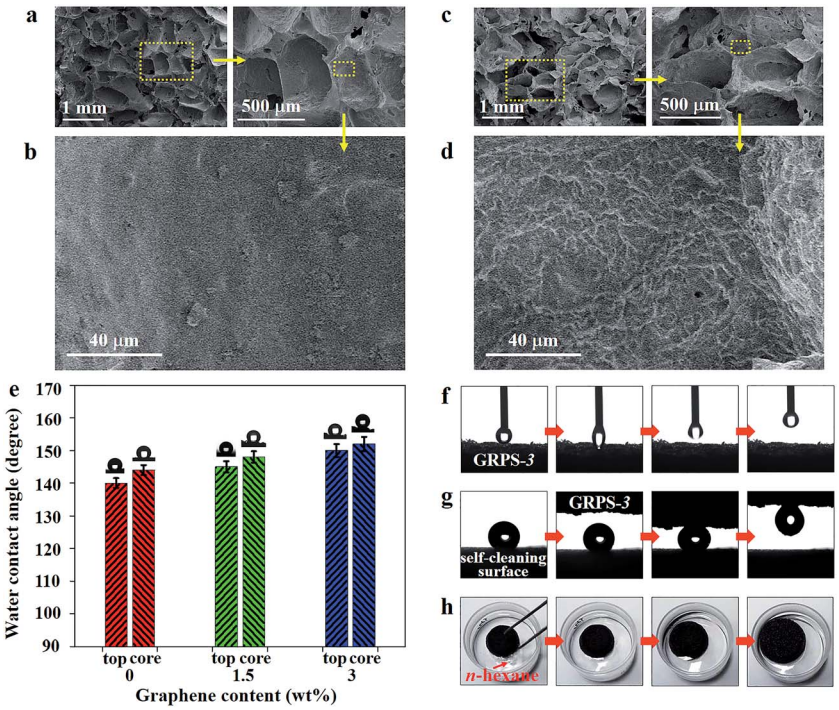

Fig. 3 Microstructures and wetting behaviors of GRPSs. (a–d) Cross-sectional SEM images of (a and b) GRPS-*0* and (c and d) GRPS-*3* at various magnifications. (e) The relationship between water contact angles and graphene loading contents in GRPSs. Internal optical images showing the shape of a water droplet (5 μL) on the surface of corresponding GRPS. (f) Sequential optical images showing the dynamic process of a water droplet in contact with the GRPS-*3* surface. (g) Transportation of a water droplet from a self-cleaning surface to the GRPS-*3* surface. (h) Dynamic swelling process of GRPS-*3* for the *n*-hexane adsorption.

water droplet is easily transferred from a self-cleaning surface (as seen in a graphene-based composite coating)[45] to the GRPS-*3* surface which served as a "mechanical hand" (Movie S3, ESI†). Additionally, GRPS-*3* could float easily on the water surface, and support water droplets to maintain their uniform spherical shapes on the GRPS-*3* surface (Fig. S5, ESI†); these characteristics are indicative of a stable superhydrophobic property. In contrast, Fig. 3h shows the expanded volume of GRPS-*3* during the *n*-hexane adsorption process (Movie S3, ESI†). The swelling ability of the cross-linked polymers is an intrinsic characteristic, which can result in a volume expansion of the polymers by adsorbing nonpolar solvents.[46] As a consequence, incorporating a low graphene content in GRPS still maintains the swelling behavior derived from a pure PDMS matrix.

PDMS sponges have been widely used as a kind of adsorbent in an oil–water separation system, due to their superhydrophobic and superoleophilic characteristics.[12] The high elasticity is beneficial for the recyclability of adsorbents and the recoverability of pollutants in practical applications. However, the adsorption of organic molecules is inefficient because of the low separation efficiency caused by the finite elastic deformation of the PDMS sponge. In this regard, incorporation of a low graphene content into the three-dimensional porous PDMS skeleton can avoid the structural damage of the nanoscale features required for super-repellency.[47] Due to its optimal mechanical feature, a PDMS sponge with graphene modification prepared by the present method can be used as an adsorbent for the removal of organic contaminations from water. Therefore, GRPS-*3* was selected as an adsorbent according to its superior elasticity and wettability (Movie S4, ESI†). As illustrated in Fig. 4a, when GRPS-*3* approached chloroform under water, the chloroform was quickly sucked out without leaving any residue. Then, when GRPS-*3* came into slight contact with the surface of an oil–water mixture, it selectively adsorbed *n*-hexane from the water surface in a few seconds (Fig. 4b). These results demonstrate that GRPSs have excellent oil-capturing ability both underwater and on the surface.

To investigate the maximum adsorption capacity (q) of as-made GRPSs, we performed adsorption tests on various organic media without any water. Fig. 4c shows the relatively high q values of GRPSs for organic liquids (3 to 19 times their own weight), which are consistent with the adsorption capacity of PDMS sponges reported in early work,[13] depending on the density, porosity and swelling ability of the polymer elastomers (Table S3, ESI†). The q values of GRPSs exhibit the same increasing order: ethanol < acetone < paraffin oil < petroleum ether < *n*-hexane < chloroform. It is known that adsorption is based on the void volume in the macropores of sponges by capillary action and is driven by the diffusion of organic molecules; thus, adsorption capacity has been reported to be linearly related to oil density.[48] Additionally, the solubility parameter (δ) plays an important role in the swelling ability of the cross-linked polymers. If the δ value of the solvent is similar to that of PDMS ($\delta = 7.3$ cal$^{1/2}$ cm$^{-3/2}$),[49] the PDMS matrix may adsorb a large amount of solvent caused by volumetric swelling (Fig. S6, ESI†). Thus, GRPSs exhibited an obvious volume change for the

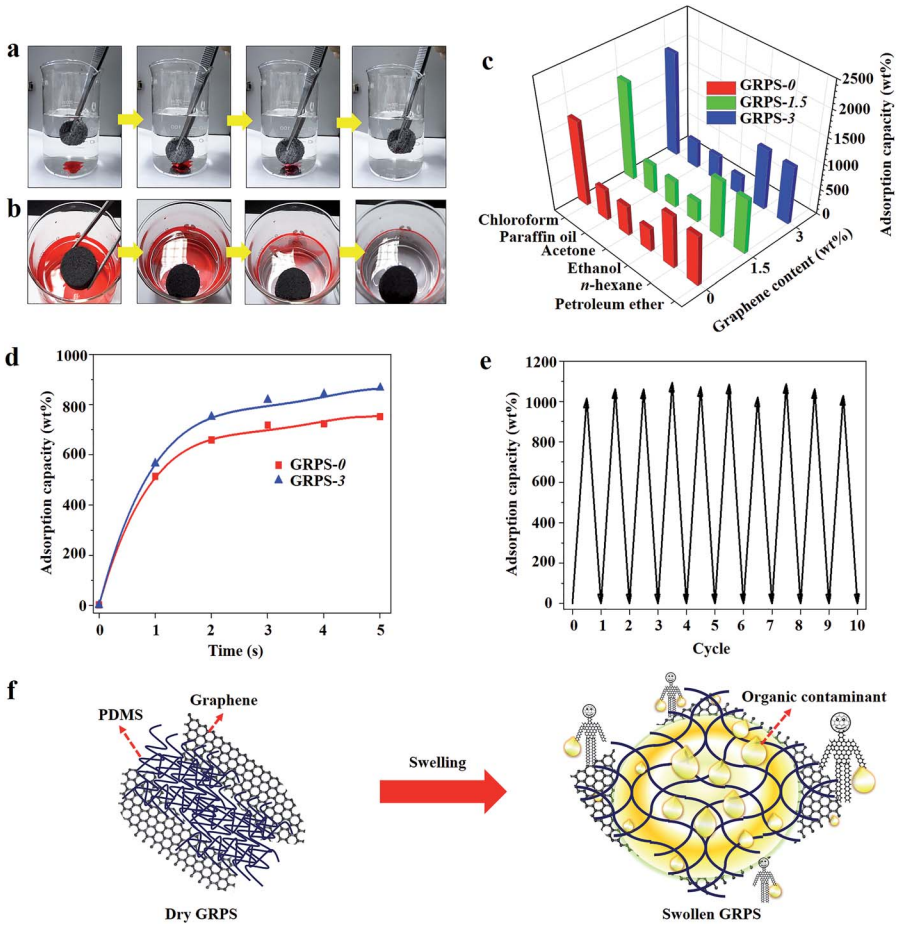

Fig. 4 Oil–water separation systems of as-prepared GRPSs. (a and b) Snapshots showing the collection process of (a) chloroform and (b) *n*-hexane (dyed by oil red 24) from water using GRPS-*3* as adsorbent. (c) Adsorption capacities of GRPS-*3* measured for a wide range of oils and organic solvents. (d) Adsorption kinetics of *n*-hexane adsorbed by GRPS-*3*. (e) Cyclic adsorption tests of GRPS-*3* for *n*-hexane. (f) Schematic illustration of a possible adsorption pathway of GRPSs with low graphene content for organic solvent.

adsorption of *n*-hexane and petroleum ether, leading to higher q values in contrast to those of ethanol and acetone. The highest q value of GRPSs for chloroform may be mainly ascribed to the highest chloroform density.

Surprisingly, the q values of GRPS-*3* were higher than those of GRPS-*0* for chloroform, *n*-hexane and petroleum ether, while the opposite trends were seen in the q values for ethanol, acetone, and paraffin oil. These phenomena are closely related to the incorporation of graphene with low content in the PDMS matrix, which may cause two opposite effects on the two types of solvents. When the solvent and PDMS matrix are compatible, the positive effect may improve the oil affinity derived from the optimal surface tension of GRPSs by graphene modification. This can be further confirmed by the adsorption kinetics. As shown in Fig. 4d, the *n*-hexane adsorption rates of GRPS-*3* were faster than those of GRPS-*0* in the first five seconds, indicating that the positive effect derived from graphene incorporation. In contrast, graphene may slightly reduce the pore size of GRPSs with an increasing graphene loading content, resulting in the restriction of the valid volume for solvent adsorption.

We measured the cyclic adsorption–squeezing experiments on GRPS-*3* using *n*-hexane as the model contaminant (Fig. 4e). After 10 cycles, Fig. 4e shows the intact structure, flexible elasticity, and high adsorption capacity of GRPS-*3*; approximately 89% of *n*-hexane was removed from the regenerated absorbent. The fluctuation of the q values in each cycle can be attributed to a small amount of organic residual that adhered to the GRPS-*3* surface. Fig. 4f further illustrates the potential adsorption pathway of GRPS with low graphene content for organic contaminants. When GRPS was immersed in solvents, the incorporation of graphene might improve the oil affinity and attract more organic molecules around the GRPS. Then, with the help of the swelling ability of the cross-linked PDMS matrix, GRPS could store the nonpolar solvents by means of the expanding volume of the interconnected network structure. Additionally, graphene might serve as a stiff scaffold to protect the PDMS matrix from mechanical damage during the swelling process, because the hard graphene nanosheets could protect the polymer elastomers from the swelling-induced modulus changes reported in the existing study.[50] Therefore, graphene nanosheets and PDMS elastomers may show a significant cooperative effect with each other in the adsorption of organic contaminants. However, the precise oil absorption mechanism of GRPS is still debatable. Thus, a detailed investigation should be carried out in the future.

Conclusions

In conclusion, we have demonstrated that a moldable clay-like unit can be transformed into an elastic PDMS sponge with a nanofiller modification *via* an ultrasound-assisted *in situ* polymerization approach. Graphene nanosheets are used as a nanofiller, PDMS as a matrix, and sea salt crystals as a template. The primary advantage of this approach is that the moderately cross-linked PDMS oligomer produces only clay-like units. Therefore, this novel composite can be molded into any desired shape *via* the elasticity and viscosity of the clay-like performance, which is especially applicable for synthesis of GRPS on a large scale. GRPS with a low graphene content exhibits high elasticity and hydrophobicity, leading to repeated adsorption of organic molecules from water. As a consequence, this approach opens up a new possibility for the efficient production of functional PDMS sponges with nanofiller modification.

Acknowledgements

This work was financially supported by the Fundamental Research Funds for the Central Universities (No. 2242016R20013), China Postdoctoral Science Foundation (No. 2016M591748), National Natural Science Foundation of China (No. 11525415, 61274114, 51420105003, 11327901, 51572296, 51372277, 11604047), and Natural Science Foundation of Jiangsu Province (No. BK20160694).

References

1 S. Bhattacharya, A. Datta, J. M. Berg and S. Gangopadhyay, *J. Microelectromech. Syst.*, 2005, **14**, 590–597.
2 L. H. Cai, T. E. Kodger, R. E. Guerra, A. F. Pegoraro, M. Rubinstein and D. A. Weitz, *Adv. Mater.*, 2015, **27**, 5132–5140.
3 P. K. Yuen, H. Su, V. N. Goral and K. A. Fink, *Lab Chip*, 2011, **11**, 1541–1544.
4 G. W. Huang, H. M. Xiao and S. Y. Fu, *Sci. Rep.*, 2015, **5**, 13971–13979.
5 S. C. Mannsfeld, B. C. Tee, R. M. Stoltenberg, C. V. H. Chen, S. Barman, B. V. Muir, A. N. Sokolov, C. Reese and Z. Bao, *Nat. Mater.*, 2010, **9**, 859–864.
6 W. L. Murphy, R. G. Dennis, J. L. Kileny and D. J. Mooney, *Tissue Eng.*, 2002, **8**, 43–52.
7 J. Yuan, X. Liu, O. Akbulut, J. Hu, S. L. Suib, J. Kong and F. Stellacci, *Nat. Nanotechnol.*, 2008, **3**, 332–336.
8 Q. Peng, Y. Li, X. He, X. Gui, Y. Shang, C. Wang, C. Wang, W. Zhao, S. Du, E. Shi, P. Li, D. Wu and A. Cao, *Adv. Mater.*, 2014, **26**, 3241–3247.
9 X. Zhao, L. Li, B. Li, J. Zhang and A. Wang, *J. Mater. Chem. A*, 2014, **2**, 18281–18287.
10 J. Chen, H. Guo, X. He, G. Liu, Y. Xi, H. Shi and C. Hu, *ACS Appl. Mater. Interfaces*, 2016, **8**, 736–744.
11 B. C. Mac Murray, X. An, S. S. Robinson, I. M. van Meerbeek, K. W. O'Brien, H. Zhao and R. F. Shepherd, *Adv. Mater.*, 2015, **27**, 6334–6340.
12 S. J. Choi, T. H. Kwon, H. Im, D. I. Moon, D. J. Baek, M. L. Seol, J. P. Duarte and Y. K. Choi, *ACS Appl. Mater. Interfaces*, 2011, **3**, 4552–4556.
13 A. Zhang, M. Chen, C. Du, H. Guo, H. Bai and L. Li, *ACS Appl. Mater. Interfaces*, 2013, **5**, 10201–10206.
14 W. R. McCall, K. Kim, C. Heath, G. La Pierre and D. J. Sirbuly, *ACS Appl. Mater. Interfaces*, 2014, **6**, 19504–19509.
15 M. C. Jung, S. H. Cho, S. H. Kim, H. Y. Kim, H. J. Lee, K. H. Oh and M. W. Moon, *Sci. Rep.*, 2015, **5**, 12908–12919.
16 J. W. Han, B. Kim, J. Li and M. Meyyappan, *Appl. Phys. Lett.*, 2013, **102**, 051903–051906.
17 D. N. H. Tran, S. Kabiri, T. R. Sim and D. Losic, *Environ. Sci.: Water Res. Technol.*, 2015, **1**, 298–305.
18 S. Liang, Y. Li, J. Yang, J. Zhang, C. He, Y. Liu and X. Zhou, *Adv. Mater. Technol.*, 2016, **1**, 1600117–1600122.
19 A. Turco, C. Malitesta, G. Barillaro, A. Greco, A. Maffezzoli and E. Mazzotta, *J. Mater. Chem. A*, 2015, **3**, 17685–17696.
20 L. Li, J. Xu, G. Li, X. Jia, Y. Li, F. Yang, L. Zhang, C. Xu, J. Gao and Y. Liu, *Chem. Eng. J.*, 2016, **284**, 78–84.
21 Z. Chen, L. Dong, D. Yang and H. Lu, *Adv. Mater.*, 2013, **25**, 5352–5359.
22 C. Lee, X. Wei, J. W. Kysar and J. Hone, *Science*, 2008, **321**, 385–388.
23 A. A. Balandin, S. Ghosh, W. Bao, I. Calizo, D. Teweldebrhan, F. Miao and C. N. Lau, *Nano Lett.*, 2008, **8**, 902–907.
24 K. S. Suslick, *Science*, 1990, **247**, 1439–1445.
25 S. J. Doicrycz and K. S. Suslick, *Science*, 1990, **247**, 1067–1069.
26 K. S. Suslick, D. A. Hammerton and R. E. Cline, *J. Am. Chem. Soc.*, 1986, **108**, 5641–5642.
27 J. Stein, L. N. Lewis, K. A. Smith and K. X. Lettko, *J. Inorg. Organomet. Polym.*, 1991, **1**, 325–334.
28 T. R. E. Simpson, B. Parbhoo and J. L. Keddie, *Polymer*, 2003, **44**, 4829–4838.
29 A. C. C. Esteves, J. Brokken-Zijp, J. Laven, H. P. Huinink, N. J. W. Reuvers, M. P. Van and G. de With, *Polymer*, 2009, **50**, 3955–3966.
30 Y. Qin, Q. Peng, Y. Ding, Z. Lin, C. Wang, Y. Li, F. Xu, J. Li, Y. Yuan, X. He and Y. Li, *ACS Nano*, 2015, **9**, 8933–8941.
31 K. J. Cha and D. S. Kim, *Biomed. Microdevices*, 2011, **13**, 877–883.
32 L. Qiu, J. Z. Liu, S. L. Y. Chang, Y. Wu and D. Li, *Nat. Commun.*, 2012, **3**, 1241–1248.
33 H. Hu, Z. Zhao, W. Wan, Y. Gogotsi and J. Qiu, *Adv. Mater.*, 2013, **25**, 2219–2223.
34 X. Gui, J. Wei, K. Wang, A. Cao, H. Zhu, Y. Jia, Q. Shu and D. Wu, *Adv. Mater.*, 2010, **22**, 617–621.
35 T. A. Schaedler, A. J. Jacobsen, A. Torrents, A. E. Sorensen, J. Lian, J. R. Greer, L. Valdevit and W. B. Carter, *Science*, 2011, **334**, 962–965.
36 J. Suhr, P. Victor, L. Ci, S. Sreekala, X. Zhang, O. Nalamasu and P. Ajayan, *Nat. Nanotechnol.*, 2007, **2**, 417–421.
37 X. Xie, Y. Zhou, H. Bi, K. Yin, S. Wan and L. Sun, *Sci. Rep.*, 2013, **3**, 2117–2122.
38 D. D. Nguyen, N. H. Tai, S. B. Lee and W. S. Kuo, *Energy Environ. Sci.*, 2012, **5**, 7908–7912.
39 D. Bodas and C. Khan-Malek, *Microelectron. Eng.*, 2006, **83**, 1277–1279.

40 K. Liu and L. Jiang, *ACS Nano*, 2011, **5**, 6786–6790.
41 L. Feng, Y. Zhang, J. Xi, Y. Zhu, N. Wang, F. Xia and L. Jiang, *Langmuir*, 2008, **24**, 4114–4119.
42 S. Wang and L. Jiang, *Adv. Mater.*, 2007, **19**, 3423–3424.
43 H. Hu, Z. Zhao, W. Wan, Y. Gogotsi and J. Qiu, *ACS Appl. Mater. Interfaces*, 2014, **6**, 3242–3249.
44 M. Jin, X. Feng, L. Feng, T. Sun, J. Zhai, T. Li and L. Jiang, *Adv. Mater.*, 2005, **17**, 1977–1981.
45 M. J. Nine, M. A. Cole, L. Johnson, D. N. Tran and D. Losic, *ACS Appl. Mater. Interfaces*, 2015, **7**, 28482–28493.
46 J. N. Lee, C. Park and G. M. Whitesides, *Anal. Chem.*, 2003, **75**, 6544–6554.
47 Z. Chu and S. Seeger, *Adv. Mater.*, 2015, **27**, 7775–7781.
48 Y. Liu, J. Ma, T. Wu, X. Wang, G. Huang, Y. Liu, H. Qiu, Y. Li, W. Wang and J. Gao, *ACS Appl. Mater. Interfaces*, 2013, **5**, 10018–10026.
49 J. N. Lee, C. Park and G. M. Whitesides, *Anal. Chem.*, 2003, **75**, 6544–6554.
50 J. W. Grate, M. Klusty, R. A. McGill, M. H. Abraham, G. Whiting and J. Andonian-Haftvan, *Anal. Chem.*, 1992, **64**, 610–624.